# Cyclotron trap

D. Gotta[1⋆] and L.M. Simons[2]

**1** Institut für Kernphysik, Forschungszentrum Jülich, D-52425 Jülich, Germany
**2** Paul Scherrer Institut, CH-5232 Villigen, Switzerland
⋆ d.gotta@fz-juelich.de

February 4, 2021

*Review of Particle Physics at PSI*
doi:10.21468/SciPostPhysProc.2

## Abstract

**The cyclotron trap was developed at SIN/PSI to increase the stopping density of negatively charged particle beams for the formation of exotic atoms in low pressure gases. A weak focusing magnetic field, produced by superconducting solenoids, is used. Particles are injected radially through the fringe field to a moderator, which decelerates them into orbits bound by the field. Further deceleration by moderators and/or low-pressure gases leads the particles to the center of the device, where they can be stopped or eventually extracted. Experiments became feasible with this technique, such as those dealing with pionic hydrogen/deuterium at SIN/PSI. Muonic hydrogen laser experiments also became possible with the extraction of muons from the cyclotron trap. The formation of antiprotonic hydrogen in low pressure targets led to successful experiments at LEAR/CERN.**

## 13.1 Introduction

The advent of meson factories in the 70's and of the antiproton factory LEAR in the 80's, resulted in a revival of interest in the physics of exotic atoms. Before then, the main focus of research was the investigation of nuclear charge parameters with muonic atoms, and the determination of the strong interaction shift and broadening in hadronic atoms [1]. Experiments had been almost exclusively performed in medium- to high-$Z$ solid or high-pressure targets. Exotic atoms were produced by decelerating the beam particles with a linear array of low-$Z$ moderators, such as $Be$, $CH_2$, or $C$ to minimize straggling.

This technique was sufficient for the purposes at that time, but was not adequate for experiments of more fundamental interest. Such experiments have in common the need of low-pressure gas targets. As an example, neutral exotic hydrogen/deuterium atoms can penetrate deeply into the field of neighbouring atoms. At higher pressures they are destroyed by the Stark effect before they can emit the X-rays one wants to measure.

A second example is given by exotic atoms of higher $Z$ formed in low-pressure gases. Here, a completely ionized electron shell can keep the exotic atom free from interactions with neighbouring atoms, thus approaching the state of an ideal exotic atom. The X-rays in question, with energies in the keV region, suffer self-absorption in high $Z$ gases. In addition, thin windows must be used. Both reasons argue against high-pressure gas targets.

Experiments planned at LEAR/CERN to measure X-rays from antiprotonic hydrogen and deuterium, motivated a new technique to stop particles at the lowest pressures. The cyclotron trap (CT I), developed and built by a group from the University of Karlsruhe working at SIN and at LEAR, met this requirement. CT I was used both at LEAR with antiprotons, and at SIN/PSI with pions and muons. A second instrument (CT II) was developed later, specially tailored to the pion and muon beams at PSI.

## 13.2 The basic principle

In the following, cylindrical coordinates are used, with $r, \theta, z$ for radius, azimuthal angle and axial direction, respectively.

The working principle of the cyclotron trap is to wind up the range path of particles inside a rotationally symmetric weak-focusing field characterized by $0 \leq n \leq 1$, where $n$ is the field index given by

$$n = -(\delta B/\delta r) \cdot (r/B) \,. \tag{13.1}$$

Particles with momenta $p_{beam}$ are injected radially through the fringe field to a radius $r_{in}$ in a direction opposite to that for ejection from a cyclotron accelerator. At this radius they are decelerated by a moderator to momenta $p_\theta$

$$p_\theta = -\frac{e}{c} B_z \cdot r_{in} \,, \tag{13.2}$$

which ideally leads to circular orbits at a given field $B_z$. A deviation from this ideal picture is caused by the injection method itself. Betatron oscillations are deliberately excited at injection for radii with $0.5 \leq n \leq 0.8$ to prevent the particles from hitting the moderator in one of the subsequent revolutions. More important is the radial spread $\Delta r_p$ caused by the momentum spread $\Delta p$ from deceleration in the injection moderator. This depends strongly on the injection scheme chosen for the different particle beams and is given by

$$\Delta r_p = r \cdot \frac{\Delta p}{p} \cdot \frac{1}{1-n} \,. \tag{13.3}$$

This leads to spreads of a few millimeters for antiproton beams at LEAR, and to a few centimeters for pion injection at SIN/PSI as the worst cases. Assuming a smooth energy loss beyond this point, the particles can then be guided by the weak focusing cyclotron field and be led to the centre of the device.

A first comparison with a linear arrangement for stopping particles with range length $R$ is given here. For a linear arrangement, the stopping process leads to a longitudinal range straggling, $\delta R$, and Coulomb scattering leads to a lateral widening of the order of $2 \cdot \delta R$. The stopping volume then is of the order of $4 \cdot (\delta R)^3$ [2]. With the cyclotron trap, the range is wound up into a spiral with its end at the center of the cyclotron trap, yielding, in first approximation, a radial spread of $\Delta r_{stop} = r_{in} \cdot \delta R/R$. The uncertainty in range leads only to an azimuthal uncertainty and multiple scattering leads to a broadening in the $z$ direction. If the deceleration is slow enough, the orbits would adiabatically follow the shrinking radius corresponding to the decreasing momentum $p$. The stopping distribution in the cyclotron trap scales with the value for the injection radius, so that a stopping volume is:

$$V_{stop}^{cyc} \propto \left( r_{in} \cdot \frac{\delta R}{R} \right)^3 \,. \tag{13.4}$$

A gain of the order of $(\frac{R}{r_{in}})^3$, compared with a linear degrader arrangement, can, in principle, be reached. In practice, the gain factor is smaller. This is caused mainly for pions by the short lifetime requiring the use of additional moderators. For pion and muon beams, losses occur during the injection through the fringe field because of the quality of the beam. In addition, range straggling in the moderator and deliberate detuning in the beginning of the deceleration process must be taken into account for all types of particles. These factors result in an additional increase of the stopping distribution.

For antiprotons, a gain factor of $10^4$ was measured. For pions and muons, gain factors of the order of 10 to 30 proved to be realistic.

## 13.3 The principle in more detail

An instructive way to visualize the principle of the cyclotron trap is given by the quasipotential picture [3,4]. The quasipotential $U(r,z)$ is given by

$$U(r,z) = \frac{1}{2m} \cdot \left( \frac{P}{r} - \frac{e}{cr} \cdot \int_0^r B_z(r',z) r' dr' \right)^2 \tag{13.5}$$

with $P$ being the so-called generalized angular momentum

$$P = r p_\theta + \frac{e}{c} \int_0^r B_z(r',z) r' dr' = \text{const} \tag{13.6}$$

Values for the quasipotential are depicted in Figure 13.1 and in Figure 13.2 for the field of CT I. Bound orbits require minima of the quasipotential curves both in radial and axial direction. This leads to the requirement $0 < n < 1$. For the minima in $U(r, z = 0)$ the radius of an orbiting particle is given by equation (13.2).

As seen from Figure 13.1, values of $P$ higher than about 6 MeV/c·m cannot lead to bound orbits as minima develop only for smaller values. The injection, e.g. of antiprotons with a momentum of 200 MeV/c, requires a momentum loss of 70 MeV/c in a moderator of suitable thickness placed at a radius of about 140 mm. In this way they are captured in a shallow potential well with $P$ slightly lower than 6 MeV/c·m. Without any further energy loss, the particles would be stopped in one of the next orbits by this moderator. If there is an additional energy loss, they eventually follow the developing potential minima. If the energy loss is sufficiently small, the particles oscillate around the newly established equilibrium radii and will be guided adiabatically to the centre of the trap. If the energy loss is too large, the centre of the device will not be included in the orbit of the particles. A negative generalized momentum would develop and the particles would even be expelled from the center [4].

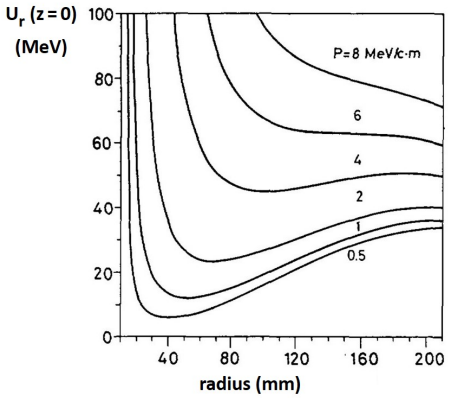


Figure 13.1: Radial distribution of the quasipotential in the median plane for different positive values of the generalized momentum $P$.

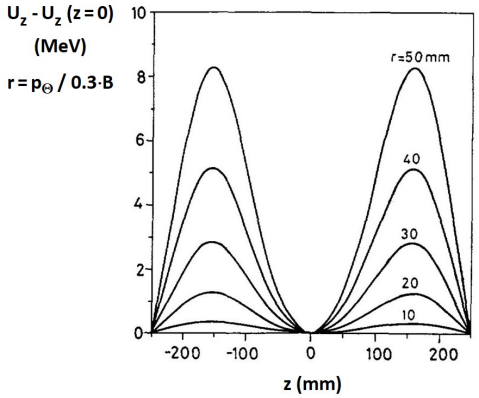


Figure 13.2: The difference of the axial distribution of the quasipotential to its value at $z = 0$ is shown for different values of the equilibrium radii $r_0$.

In the axial direction the focusing is very strong in the beginning of the deceleration process, and decreases when the particles orbit to the center of the cyclotron trap. They will be stopped at short axial distances from the center because of their low energy. In addition the magnetic mirror effect will contain them axially. Applying an axial electric field would provide the opportunity to extract them to form a particle beam.

## 13.4 Phase space considerations

The phase space development in the case of energy loss is described by the extended Liouville theorem [5]. For the deceleration of particles in matter the dissipative force given by the energy loss (Bethe-Bloch formula) can be approximated as a function of the momentum $p$ by

$$Q \propto p^{\alpha(p)} \,. \tag{13.7}$$

The value of $\alpha$ varies between $-1.4$ and $-1.7$ for materials with low ionization potentials. Assuming $\alpha$ is piecewise constant, and partitioning the deceleration path into constant time intervals, the ratio of the momentum spread at the beginning (i) and the end (f) of an interval is given by:

$$\frac{\Delta p_f}{\Delta p_i} = \left(\frac{p_f}{p_i}\right)^{\alpha}. \tag{13.8}$$

This relation does not hold if the emittance changes during deceleration, as is the case for the deceleration by an electric field. Energy loss, however, applies equally in any spatial direction resulting in a constant emittance. Going from linear to circular motion, we arrive at an expression that is central for understanding the working principle of the cyclotron trap

$$\frac{\Delta p_f}{\Delta p_i} = \left(\frac{p_f}{p_i}\right)^{\alpha} \cdot \frac{\omega_i}{\omega_f} \tag{13.9}$$

with $\omega$, the circular frequency of motion, being proportional to the magnetic field strength. The increase of $\Delta p$, caused by the momentum decrease, is partially counteracted by the increase of the cyclotron frequency at smaller radii. The interesting quantity for the formation of exotic atoms, however, is the radial spread $\Delta r_p$. It is connected to the momentum spread via equation (13.3). For the orbits with small radii and $n$ approaching a value of 0, a decrease of $\Delta r_p$ can be expected.

Extensive calculations of the dynamics of the injected and decelerated particles with real beam parameters and the geometry of the finally-built cyclotron traps confirmed these expectations. The radial extension of the stopping distribution corresponds to the radial spread of the beam at the beginning of the deceleration process. The axial extension of the stopping distribution, however, is almost a factor of 2 bigger than the axial extension at the beginning.

## 13.5 Technical realisation

The weak focusing field is produced by two superconducting ring coils. Because of the high field strength, the dimensions of the device can be kept small. The field direction is horizontal so that the particle orbits are in the vertical plane. Access to the stopping region is provided by a borehole in the cryostat housing of the coils. We describe here the set-up of CT II shown in Figure 13.3 and Figure 13.4.

The two superconducting coils are located in separated cryostats. They are surrounded by a soft iron return yoke that also serves as magnetic shielding to reduce the field at a radius of 29.5 cm. Additional soft iron pieces are mounted at the inner cryostat walls to optimize the field. Iron rings are mounted to balance magnetic forces. Beams are injected through a hole in the shielding as shown in Figure 13.4.The two halves can be separated to access the interior, thus providing a high versatility.

## 13.6 Particle physics experiments

As most of the experiments performed with the two cyclotron traps were discussed in a review paper by D. Gotta [6] including extensive references, the following discussion can be brief.

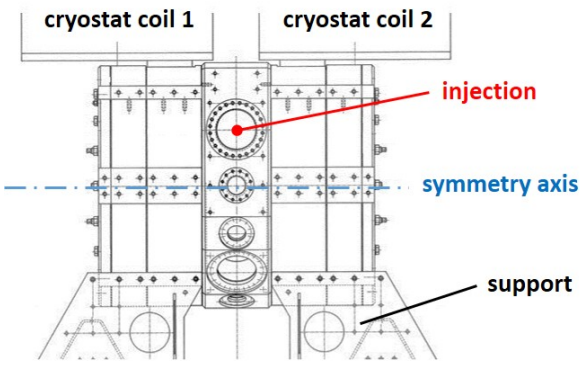


Figure 13.3: The set-up of CT II. The magnetic field is horizontal with the injection point in the vertical symmetry plane, about 200 mm from the symmetry axis. The supporting table and the two separated cryostats are indicated.

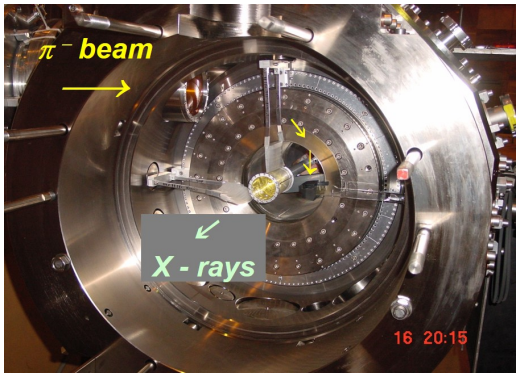


Figure 13.4: The interior part of CT II with one of the two halves removed. The beam enters from the left and is guided to a gas target on the symmetry axis with the help of additional moderators.

### 13.6.1 Antiprotonic atoms

The possibility of experiments with antiprotonic atoms at LEAR/CERN motivated the construction of the cyclotron trap CT I. The 105 MeV/c antiproton beams were ideal for the deceleration with the cyclotron trap. 86% of the incoming beam can be stopped in a 30 mbar hydrogen gas target with a diameter of 20 mm (FWHM). This resulted in an increase of stopping densities of more than 4 orders of magnitude, and led to successful measurements of the ground state shift and width in antiprotonic hydrogen isotopes. A measurement of these quantities for the $2p$-state in these atoms with a crystal spectrometer was also made [7].

### 13.6.2 Muonic and pionic atoms

The muon and pion beams at SIN/PSI presented considerable difficulties for the use of the cyclotron trap. The emittance of the beams and the lifetimes of the particles, deviated from the ideal situation encountered with antiprotons. Nonetheless, experiments with the first cyclotron trap (CT I) proved to be successful. In a first experiment, the pion mass was determined from pionic atoms formed in nitrogen gas with an almost depleted electron shell [8]. Earlier experiments suffered from the lack of knowledge of the state of the electron shell, as a solid Mg target was used. The determination of the pion mass was later improved by using CT II, allowing for energy calibration with muonic oxygen [9] (Section 10 [10]). Coulomb explosion was directly observed for the first time; this occurs in the formation of exotic atoms from molecules such as $N_2$ [11]. A first round of crystal spectrometer measurements of X-rays in pionic hydrogen isotopes was also performed. The work with muonic atoms led to the observation of the two-photon transition in muonic boron [12].

The second cyclotron trap (CT II) was developed to adapt its acceptance to the emittance of the pion and muon beams at PSI. For pions, about 1% of the initial beam could be stopped in a hydrogen target at STP. For muon beams, this number is about an order of magnitude higher. This led to a successful series of measurements in muonic hydrogen and in both pionic hydrogen and deuterium, reducing typical measuring times to a month (Section 14 [13]). The line shape of the muonic hydrogen $K\alpha$ transition was determined with high precision as a prerequisite for later experiments in pionic hydrogen [14]. A method was developed to extract muons from the center of the trap to form a low-energy muon beam. This opened a path for important experiments to determine the proton radius [15] (Section 21 [16]).

## 13.7 Atomic physics experiments

### 13.7.1 Ionized exotic atoms

It became clear at an early stage that the possibility of forming exotic atoms in low pressure gases can lead to a complete ionization of the electron shell [17]. After formation, the electromagnetic cascade depletes the electron shell up to $Z = 36$ for antiprotons, and up to $Z = 18$ for muons or pions. As the natural linewidth of the corresponding transitions is negligibly small, these X-rays can be used for calibration of some particle physics experiments. The atomic physics aspect of these experiments proved to be interesting by itself [18, 19].

### 13.7.2 ECR-source: a by-product

The crystal spectrometer experiment in pionic hydrogen and deuterium required a precise knowledge of the response function of the device. To achieve this, the of geometry CT II was changed to that of an ECR source providing a high-intensity X-ray source. Here the distance of the solenoids had to be changed and a hexapole was inserted on the axis of CT II [20]. Then, the crystal spectrometer could be calibrated in a set-up equivalent to the pionic and muonic experiments [21].

## References


[1] C. W. J. Hüfner, F. Scheck, *Muon physics I*, Academic Press, New York (1977).

[2] L. Simons *et al.*, *Exotic atoms and their electron shell*, Nucl. Instr. and Meth. B **87**, 293 (1994).

[3] A. N. L. A. A. Kolomensky, *Theory of Cyclic Accelerators*, North-Holland Publishing Company, Amsterdam (1966).

[4] L. M. Simons, *Recent results on antiprotonic atoms using a cyclotron trap at LEAR*, Physica Scripta **T22** (1988).

[5] A. J. Lichtenberg, *Phase space dynamics of particles*, J. Wileys, New York (1969).

[6] D. Gotta, *Precision spectroscopy of light exotic atoms*, Progr. Part. Nucl. Phys. **52**, 133 (2004).

[7] D. Gotta *et al.*, *Balmer α transitions in antiprotonic hydrogen and deuterium.*, Nucl. Phys. A **660**, 283 (1999).

[8] M. Trassinelli *et al.*, *Measurement of the charged pion mass using X-ray spectroscopy of exotic atoms*, Phys. Lett. B **759**, 583 (2016).

[9] S. Lenz *et al.*, *A new determination of the mass of the charged pion*, Phys. Lett. B **416**, 50 (1998).

[10] M. Daum and D. Gotta, *The mass of the $\pi^-$*, SciPost Phys. Proc. **2**, ppp (2021), doi:10.21468/SciPostPhysProc.2.XXX.

[11] T. Siems *et al.*, *First direct observation of Coulomb explosion during the formation of exotic atoms*, Phys. Rev. Lett. **84**, 4573 (2000).

[12] K. Kirch *et al.*, *Metastability of the muonic boron 2s state*, Phys. Rev. Lett **78**, 4363 (1997).

[13] D. Gotta and L. Simons, *Pionic hydrogen and deuterium*, SciPost Phys. Proc. **2**, ppp (2021), doi:10.21468/SciPostPhysProc.2.XXX.

[14] D. Covita *et al.*, *Line shape analysis of the $K\beta$ transition in muonic hydrogen*, Eur. Phys. J. D **72**, 72 (2018).

[15] A. Antognini *et al.*, *Proton structure from the measurement of the $2s-2p$ transition frequencies of muonic hydrogen*, Science **339(6118)**, 417 (2013), doi:10.1126/science.1230016.

[16] A. Antognini, F. Kottmann and R. Pohl, *CREMA*, SciPost Phys. Proc. **2**, ppp (2021), doi:10.21468/SciPostPhysProc.2.XXX.

[17] R. Bacher *et al.*, *Muonic atoms with vacant electron shells*, Phys. Rev. Lett. **54**, 2087 (1985).

[18] D. Gotta *et al.*, *X-ray transitions from antiprotonic noble gases*, Eur. Phys. J. D **47**, 11 (2008).

[19] K. Kirch *et al.*, *Muonic cascades in isolated low-$Z$ atoms and molecules*, Phys. Rev. A **59**, 3375 (1999).

[20] S. Biri *et al.*, *Electron cyclotron resonance ion trap: A hybrid magnetic system with very high mirror ratio for highly charged ion production and trapping.*, Review of Scientific Instruments **71**, 1116 (2000).

[21] D. F. Anagnostopoulos *et al.*, *On the characterisation of a Bragg spectrometer with X–rays from an ECR source.*, Nucl. Instr. and Meth. A **545**, 217 (2005).